Fuel 307 (2022) 121776

Contents lists available at ScienceDirect

Fuel

journal homepage: www.elsevier.com/locate/fuel

Full Length Article

Higher-order compositional simulation of asphaltene damage and removal in the wellbore by the CPA-EOS

Ali Zidane [a], Abbas Firoozabadi [a,b,*]

[a] Reservoir Engineering Research Institute, Palo Alto, CA, USA
[b] Department of Chemical and Biomolecular Engineering, Rice University, Houston, TX, USA

ARTICLE INFO

Keywords:
Asphaltene formation damage
Multiphase flow
Equation of state
Cubic-plus association
Compositional simulation

ABSTRACT

Simulation of asphaltene damage around the wellbore is important in relation to well productivity. Existing numerical approaches rely on the surface adsorption of asphaltene on the rock using a Langmuir isotherm. We demonstrate that asphaltene accumulation around the wellbore can be modeled as an asphaltene-rich liquid phase without the need to include surface adsorption explicitly. The relative permeability concept accounts for surface adsorption as well as pore-plugging. Our approach is fully verified with recent experimental data. This work is based on the fact that below the asphaltene onset pressure, an asphaltene-rich phase is formed with much higher viscosity than the oil phase from which it evolves. We perform phase behavior calculations using the cubic-plus association equation of sate (CPA-EOS). Flow and species transfer between the phases are simulated based on the higher-order method with high accuracy and low numerical dispersion. The algorithm includes full 3D unstructured gridding to model well damage and frequency and extent of asphaltenes removal in field scale applications. An example with a fracture crossing the producing well is included to examine deposition in the fracture and the matrix.

1. Introduction

Asphaltenes precipitate around the wellbore due to pressure drop and/or change in composition from injection of CO_2 and other gases. The region of precipitation in a production well expands into the formation. The precipitated asphaltene phase has a low mobility and its saturation build-up results in loss of well productivity and may eventually kill the well unless solvents are used to remove the precipitated phase. The precipitated asphaltene phase has a high content of asphaltenes. Asphaltenes are soluble in aromatics such as benzene, toluene, and xylenes. These aromatics are often used to clean the well and wellbore areas [1].

Asphaltene precipitation is frequently interpreted as permeability reduction and alteration of rock wettability (Buckley 1995). The reduction of absolute permeability may not have a sound basis, as we will discuss later. The asphaltene precipitation in depletion results mainly from the effect of pressure drop around the wellbore. In fluid injection, a change of composition is the main cause, and precipitation may occur in the entire formation [2–4]. As we will show in this work, there are major differences between the asphaltene accumulation in the injector and in producing wells.

The majority of authors in the literature model asphaltene flow damage based on adsorption. Nghiem et al. [5] consider the deposited asphaltenes as a solid phase. A compositional model is used based on the Peng-Robinson (PR) equation of sate (EOS). Asphaltene deposition is described by adsorption from the Langmuir isotherm (Nghiem et al. 1998). A three-phase oil/gas/solid flash calculation provides saturations in oil, gas, and solid phases [5]. The equilibrium in Nghiem et al. [5] is based on the equality of fugacity for all components in the oil and gas phases and the equality of fugacity of the solid (asphaltene) to the fugacity of the same component in the oil phase. The fugacities (except for the solid) are calculated by the EOS. The fugacity of the pure solid is calculated as a function of pressure, temperature, molar volume, and a reference fugacity. Kohse and Nghiem [6] extend the work of Nghiem et al. [5]. They divide the asphaltenes into two solids. One solid consists of small particles that can flow with the oil phase, and the second solid consists of larger aggregates that may deposit on reservoir rock. A reversible chemical reaction is provided that describes the transformation from the first solid to the second solid. A surface deposition rate coefficient is used which depends on rock type to describe

* Corresponding author.
E-mail address: af@rerinst.org (A. Firoozabadi).

https://doi.org/10.1016/j.fuel.2021.121776
Received 15 May 2021; Received in revised form 18 August 2021; Accepted 19 August 2021
Available online 26 August 2021

asphaltene deposition [6]. Wang and Civan [7] have investigated the damage by asphaltene deposition in the formation. They describe the asphaltene precipitation by a polymer solution model that uses the asphaltene solubility parameter. They further assume that the asphaltene component is either soluble in the oil phase (based on polymer solubility concept) or deposited on the rock surface. Wang and Civan [7] assume that the asphaltene deposition rate is a function of interstitial velocity of the oil phase. Once deposited, the pore-throat is reduced by the amount of deposited asphaltenes. Behbahani et al. [8] have proposed an extension of the Wang and Civan's [7] approach to model asphaltene deposition based on two mechanisms. One mechanism is surface adsorption described by the Langmuir isotherm; the other mechanism is pore plugging. Asphaltene deposition from mechanical plugging occurs when the size of the asphaltene aggregates become larger than the pore throat; the deposition rate due to mechanical plugging in Behbahani et al. [8] is related to pore throat diameter. The authors propose a method to measure the deposited asphaltenes attributed to different mechanisms (adsorption and mechanical plugging) using cyclohexane and toluene reverse flooding. They calculate the effective permeability from pressure drop and perform experiments to restore the permeability. They report that 60–80% of the total damage is due to mechanical plugging whereas adsorption contributes 20–40% of the total permeability reduction.

Recently, Mohebbinia et al. [9] and Abouie et al. [10] present simulation of the process following the adsorption formulation using a Langmuir isotherm. In addition to adsorption, the authors include mechanical entrapment. They use the PC-SAFT EOS [11] for phase behavior calculations.

Asphaltene precipitation is thermodynamically reversible, and the asphaltene species can dissolve in the asphaltene-rich phase and the oil phase. Asphaltene adsorption layer is generally governed by the molecular interactions between the surface molecules and the adsorbed molecules. The thickness of the strong adsorbed layer is generally less than 1 nm and can hardly exceed 2 nm even when there is a weak second and third layer [12]. When molecular structured are formed on the surface by heteroatoms, the thickness may not exceed 3 nm [13]. When the deposited layer is of the order of 4 nm or more a thin liquid film is formed over the surface. This is no longer referred to adsorption. In appendix A we show the composition of three phases in a three-phase mixture of gas, oil, and asphaltene-rich phase. In the same Appendix, the amount of asphaltenes in the asphaltene-rich liquid phase from pressure drop in a light oil and from mixing of the stock tank oil (STO) and heptane are also presented. There is a vast difference of the asphaltene content in the asphaltene-rich phase. The asphaltene in the former is around 40 wt% or less. The asphaltene content of the latter is around 70 wt%. The phase with the lower asphaltene content is expected to flow readily.

In a departure from an adsorption-type and pore-plugging model, Nasrabadi et al. [14] assume an asphaltene-rich liquid phase which can fully describe asphaltene damage in porous media. The authors use the cubic-plus-association (CPA) EOS for phase behavior calculations. Three hydrocarbon phases might coexist based on the thermodynamic conditions, where two of the phases are in liquid state and a third is a gas phase. The asphaltene-rich liquid phase appears at a pressure between the upper and lower asphaltene onset pressures. In [15], the authors show that in both lab and field scale when the oil injection rate increases the asphaltene phase flows.

This work is based on the CPA-EOS. The algorithm accounts for three hydrocarbon phases: one gas phase and two liquid phases with one rich in asphaltenes. We use the term "oil phase" interchangeably with "light liquid phase" and "light oil phase." The relative permeability concept accounts for surface adsorption. When asphaltene onset point is reached and the asphaltene-rich phase forms, its mobility is very low. The critical saturation of asphaltene-rich phase and the relative permeabilities describe the asphaltene formation damage process.

The description of formation damage by asphaltenes requires an accurate well representation. A simplified point sink/source well representation may not properly describe the physics of asphaltene damage near and/or at the wellbore. In this work we present a realistic representation of well geometry in modeling of asphaltene precipitation. The numerical discretization is based on fully unstructured grids and the hybridized mixed finite element [16–18]. The mass balance equations in our model are discretized with the mass conservative discontinuous Galerkin method (DG) and an implicit pressure explicit concentration (IMPEC) scheme is used in the temporal discretization [19–24].

2. Methodology

The main parameters which describe the flow of the asphaltene-rich liquid phase are relative permeability endpoints, Corey exponents, and residual saturations (in case of asphaltene-rich liquid phase, due to formation of new phase the critical saturation may define it more precisely). Surface adsorption and mechanical plugging are part of the relative permeability in our simulations. Adopting this approach for modeling asphaltene deposition reduces the complexity of the algorithm and the computational cost. It is also consistent with the relative permeability concept. It does not double-count adsorption and small pore plugging. It is rigorous without depending on the empirical formulations that are usually used for modeling of adsorption and mechanical entrapment. We have carried out core flood testing in single phase with a crude oil and decane. Both fluids give the same permeability. The fluid used does not affect permeability. Molecular dynamic simulations show there are often only one or two adsorption layers. Relative permeability in two-phase flow accounts for adsorption. In our model, the asphaltene-rich phase is a liquid phase that has a high viscosity. The low mobility of the asphaltene-rich liquid phase and, when coupled with the residual saturation, the relative permeability fully describes the displacement and/or small pore plugging phenomena. Three-phase relative permeabilities are evaluated based on Stone's model [25–27]. We would like to point out that formation of asphaltene-rich liquid phase is like formation of condensate liquids in gas production [28]. There are upper dew points and there may exist a lower dew point. In asphaltene phase formation, there may be also upper and lower onset points. In gas condensates, the saturation at which liquid condensate flows is termed the critical condensate saturation. The saturation at which the asphaltene-rich liquid starts to flow can be referred to more precisely as the critical asphaltene-phase saturation. The same behavior in critical saturation is also observed even in gas phase formation in porous media and the gas becomes mobile after reaching a critical saturation. This aspect is key in relation to high recovery in cold production from heavy oils [29]. To comply more with the conventional terminology, we may refer to it as the residual asphaltene phase saturation.

In the numerical model, a stability analysis is performed to determine whether an element is in single or in multi-phase, based on pressure, temperature, and composition. If unstable, phase-split calculations (referred to as flash) are performed to determine phase densities and compositions. The calculations are based on the assumption of local thermodynamic equilibrium (the equality of fugacities of each component in all phases). The phase with the highest amount of asphaltenes is the asphaltene-rich liquid phase. There is no issue in phase tracking and phase identification.

3. Results and discussion

3.1. Verification with laboratory measurements

We first verify the algorithm with a comprehensive set of measurements from Mohammadzadeh et al. [30]. The authors [30] report detailed compositional analysis, asphaltene onset pressure, bubble point pressure in two-liquid phase state, viscosity and density measurements. These data are valuable in CPA-EOS parameter estimation and in

Table 1
Oil composition representation in our simulations: Lab scale verification.

Component	Mole fraction
N_2-C_1	0.39849
CO_2- C_2	0.05177
C_3-C_4	0.09728
C_5-C_6	0.06362
C_7-C_8	0.07248
C_9-C_{10}	0.05409
Heavy fraction	0.259643
Asphaltene	0.002627

Table 2
Critical point and other relevant data and the CPA-EOS parameters: Lab scale verification.

T_c(K)	P_c(bar)	Acentric factor	Molar weight (g/mol)	Component
190.20	45.92	0.01	16.06	N_2-C_1
305.29	49.16	0.10	30.34	CO_2- C_2
391.85	40.36	0.17	50.08	C_3-C_4
491.44	33.43	0.25	79.21	C_5-C_6
559.65	28.67	0.33	105.27	C_7-C_8
630.48	26.16	0.41	131	C_9-C_{10}
845.70	11.40	0.99	318	Heavy fraction
1274	6.8	1.75	1800	Asphaltene

Association volume: 0.01; Association energy for asphaltene-asphaltene: 2000 K; Association energy for asphaltene-resin: 500 K

viscosity verification in single oil phase. The authors design their experiments such that they have features similar to depletion in a large formation. The work can serve in examination of the asphaltene models and allow discussion of widespread inconsistencies in the literature, especially related to the practice of effective permeability reporting instead of pressure drop reporting. Mohammadzadeh et al. [30] report live oil injection in a tube. The tube is sand packed to form a porous medium of 55 md permeability and a porosity of 19%. The length of the tube is 60 feet. Injection and production are performed at constant pressures. We simulate the experiments in 1D with 500 grids. The composition of the live oil extended to C_{30+} is reported by Mohammadzadeh et al. [30]. In this work we limit the oil description to C_{11+}. The properties of C_{11+} (critical temperature, pressure, acentric factor) are adjusted to match the properties of the oil. The heaviest component (C_{11+}) is further divided into two components: the asphaltenes and the heavy fraction. The live oil composition is shown in Table 1 and the EOS parameters are shown in Table 2. We use part of pressure data to estimate Corey's exponent in the relative permeability for the oil phase and the residual oil saturation to the asphaltene-rich liquid phase. A Corey's exponent of 2.85, and a residual saturation of 20% are used for the oil phase in this example. The critical saturation of the asphaltene rich liquid phase is set to 10% and an endpoint relative permeability of 0.2 and a Corey's exponent of 2 are used for the asphaltene-rich phase. We have used part of the data from the experiment (pressure and rate) to obtain Corey's exponents and residual saturations. The flow in this example is in two-phase with the exception of the last part of the experiment in asphaltene deposition measurements. The 10% critical asphaltene-rich phase saturation is partly based on experimental observations, which will be discussed. Note that the exponent of the asphaltene-rich liquid is less than the oil phase, as expected. The asphaltene-rich liquid phase is the more wetting phase compared to the oil phase. In simulation of the experiment in [30] we only need the relative permeability of the oil phase and the asphaltene-rich liquid phase. In depressurization to atmosphere pressure to infer asphaltene phase saturation and measured asphaltene content along the core length, the relative permeability of all three phases is required. Three-phase flow calculations are carried out to determine the final asphaltene in the core reported in [30].

The saturation (bubble point) pressure of the oil is 197 bar and the asphaltene onset pressure (AOP) is 345 bar. All measurements are at a

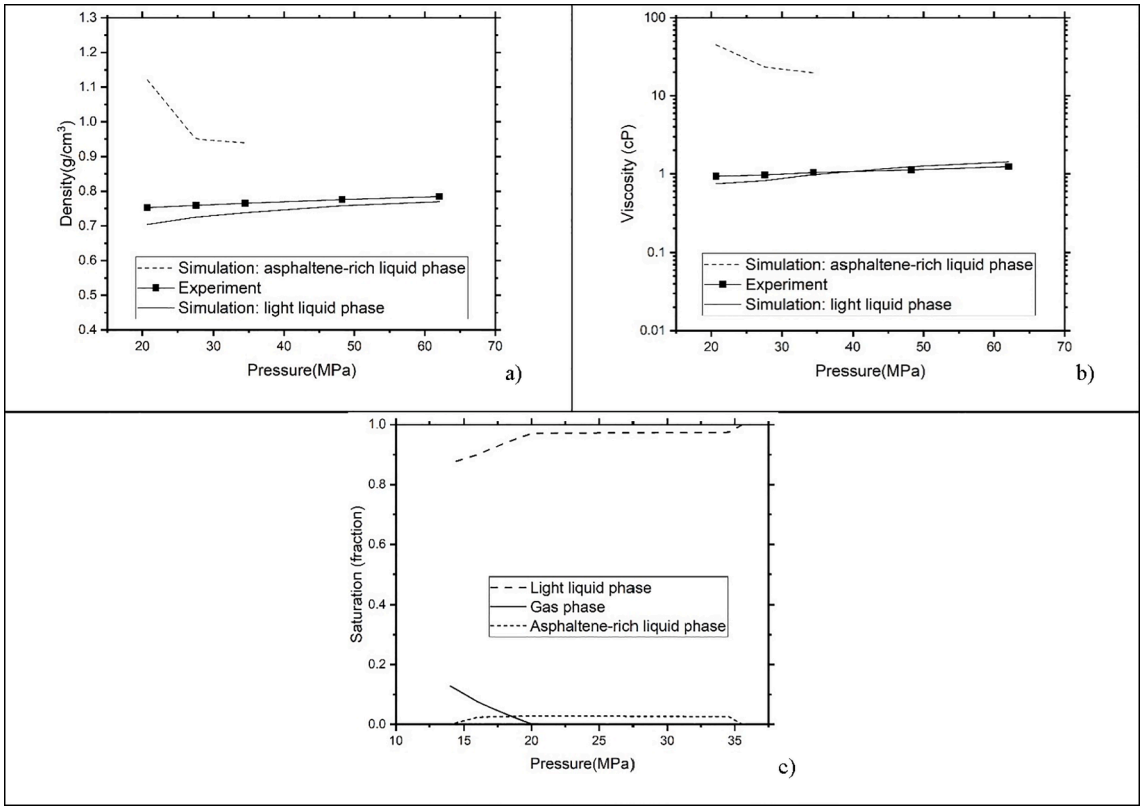

Fig. 1. Density (a), viscosity (b), and phase saturation (c), vs. pressure: Lab scale verification.

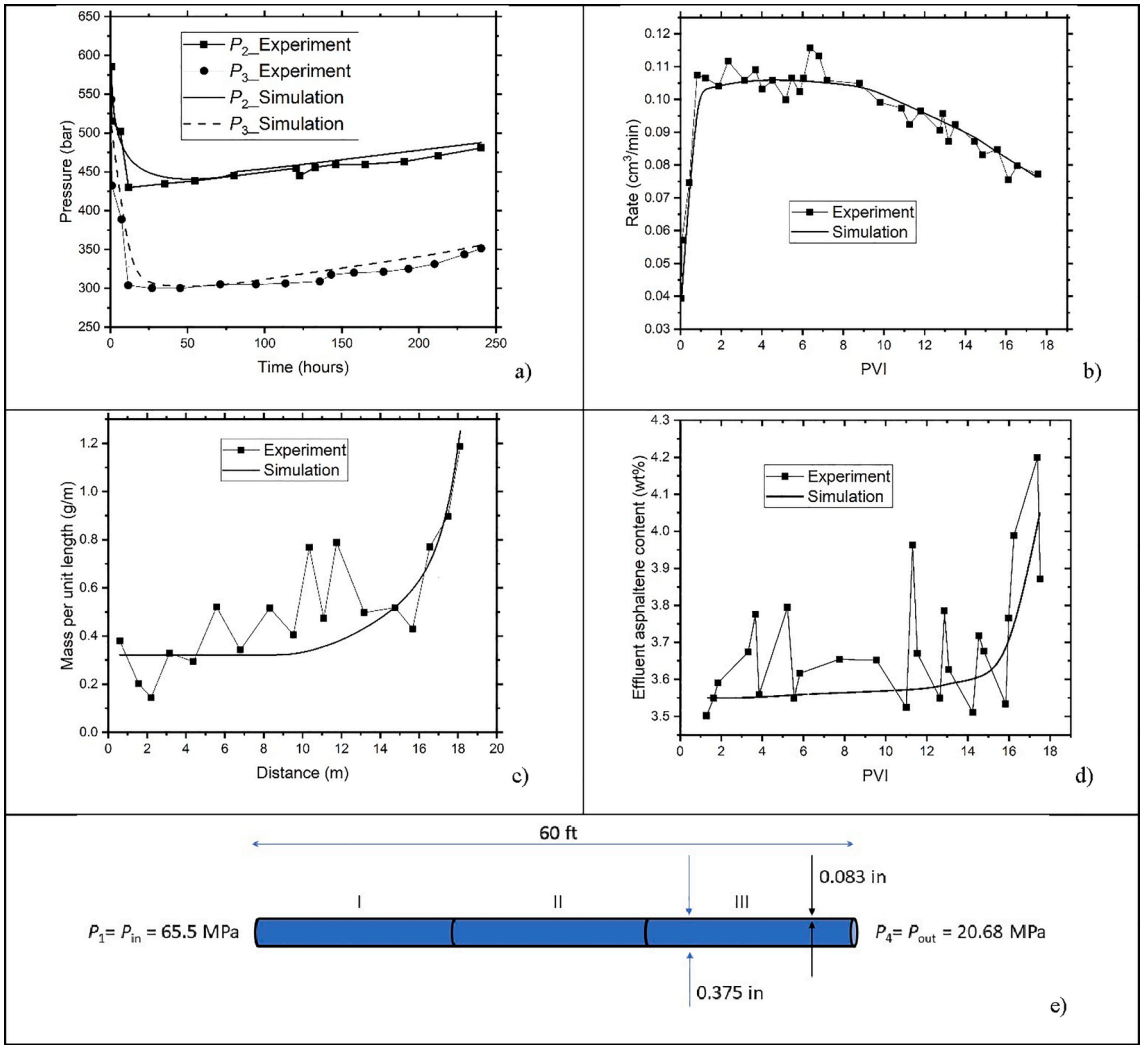

Fig. 2. Pressure vs. time (a), injection rate vs. PVI (b), asphaltene content in mass per unit length vs. distance (c), effluent asphaltene content vs. PVI (d), and sketch of the setup (e): Lab scale verification.

temperature of 93.3 °C. The density and viscosity of oil in our characterization are compared to experimental data at different pressures and results show a good agreement as seen in Fig. 1(a, b). In addition, we present in Fig. 1c the saturation envelope showing the three phases (oil phase, asphaltene-rich phase, and gas phase). Note that results in our calculations are for two-phase (below the asphaltene onset pressure), the oil phase and the asphaltene-rich liquid phase as opposed to the experimental measurements where asphaltene-rich phase is dispersed in the oil phase at short time intervals of measurements. Above the onset pressure there is no asphaltene-rich phase.

The duration of injection is 250 h, the equivalent of injecting 18 PV of live oil. Mohammadzadeh et al. [30] report pressure changes at 20 feet (designated as P_2) and 40 feet (designated as P_3) versus time. Note that P_1 and P_4 are pressure at the inlet and outlet and are kept constant during the experiment. In Fig. 2a we show the comparison of P_2 and P_3 from our simulations to the experimental data. A good agreement is observed. Injection at constant pressure implies a variable injection rate that is reported in [30]. In Fig. 2b we compare the injection rate from our simulation to the experimental data.

At the end of injection, we reduce the pressure to one atmosphere to determine the amount of asphaltenes across the core. Mohammadzadeh et al. [30] have measured the asphaltene content of both the oil phase and the asphaltene-rich liquid phase along the tube at one atm. In our simulations we first assume injection and production are zero (corresponding to closing of inlet and outlet valves), then we perform a stepwise decrease of the pressure at the outlet. In Fig. 2c we show the asphaltene mass per unit length from our simulations and the experimental data. Results presented in Fig. 2c are at the end of the simulation, and after reaching atmospheric conditions. At this stage, the total number of grids within one-meter length are grouped together and the total mass of asphaltene from both phases (light oil phase and asphaltene-rich phase) is calculated. A clear observation from Fig. 2c is that there is no meaning to effective permeability of the whole tube. Most of the tube will be free for asphaltene deposition. Deposition will only occur in the segment below the AOP of 345 MPa. Fig. 2d shows the effluent asphaltene content versus PVI. The effluent asphaltene content is calculated from the asphaltene content in the oil phase in addition to the asphaltene-rich liquid phase. Results presented in Fig. 2 demonstrate the accuracy of the proposed algorithm.

Mohammadzadeh et al. [30] conduct their experiment for a period of 250 h. In our simulations we have extended the simulation time to 500 h. Simulation results show a further increase in pressure at points 2 and 3 (P_2, P_3) and a pronounced decrease in injection rate (Fig. 3a,b). The pressure at points 2 and 3 and injection rate to 500 h, as well as asphaltene-rich phase saturation, are shown in Fig. 3. The amount of asphaltene-rich liquid phase produced to 25 PVI might have been small due to very low mobility. At lower pressures, the viscosity is higher. During depletion, the viscosity will increase substantially more, further

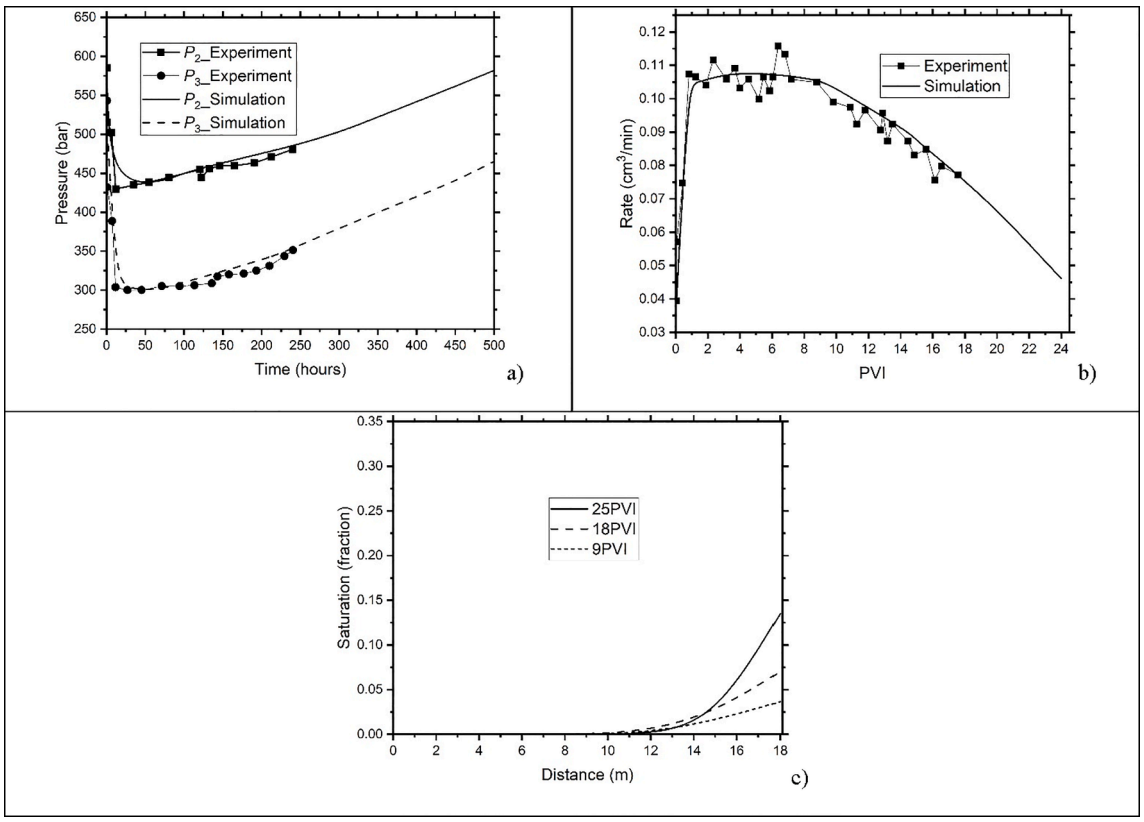

Fig. 3. Pressure vs. time (a), injection rate vs. PVI (b), and saturation of asphaltene-rich liquid phase vs. distance (c). The experiment is conducted to 250 h (18 PVI): Lab scale verification.

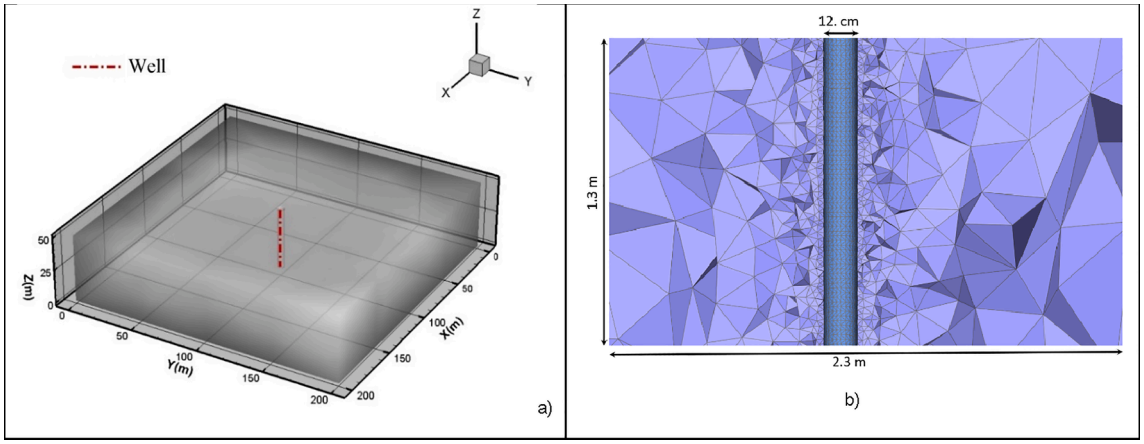

Fig. 4. Domain (a), and a cross-section showing discretization grids near well region (b): Depletion example.

reducing the mobility of the asphaltene-rich liquid phase. In measuring density and viscosity below the upper AOP, the authors report the values for the mixture of the oil phase and the asphaltene aggregates suspended in the oil phase. It will take substantial time for the asphaltene aggregates to separate from the oil phase [31]. In our CPA-EOS calculations, our density and viscosity results are based on two separate phases. This distinction is not made in the measurements because sufficient time was not allowed for phase segregation. In many studies in phase behavior of live oils, phases are separated [32].

We like to point out that in all of our calculations, we do neglect supersaturation in phase change. The only condition which supersaturation may be important is the region far from the well. In that region, since the amount of asphaltene-rich liquid phase is low, the effect on recovery and well performance may be negligible.

3.2. *Reservoir scale depletion and asphaltene precipitation and removal around the well*

In our first large scale simulation, we investigate asphaltene deposition by depletion at a constant well production rate and examine asphaltene saturation buildup around the wellbore. We consider a domain with dimensions of 200 × 200 × 50 m^3, 20% porosity, and 50 md permeability. The oil composition and the temperature are the same as in the lab scale example. The relative permeability parameters are also kept the same except for an endpoint relative permeability of 0.4 for the oil phase because we include connate water. In the lab scale, connate

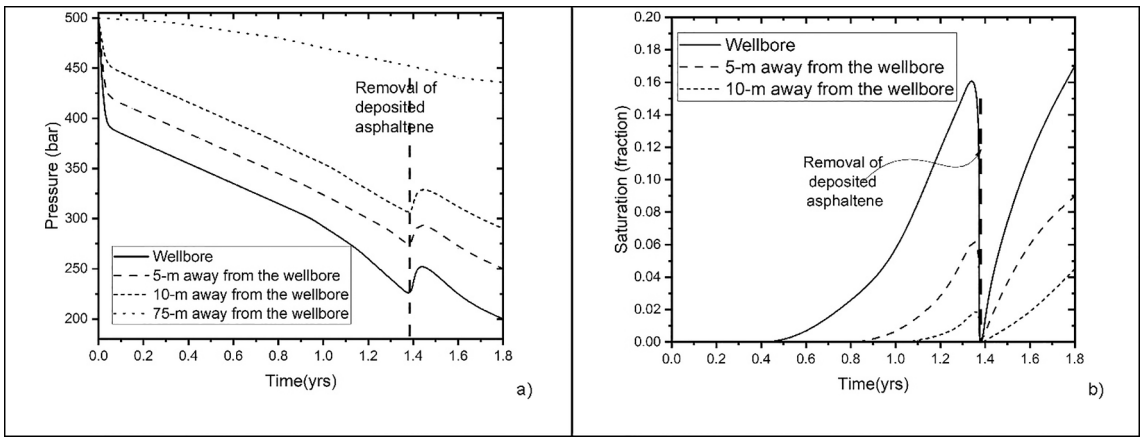

Fig. 5. Pressure vs. time (a) and saturation of asphaltene-rich liquid phase vs. time (b) at different distances from the well. The simulation results are based on gradual increase of the rate of production in a period of two weeks. At 1.37 yrs, the same process is repeated for a period of 10 days: Depletion example.

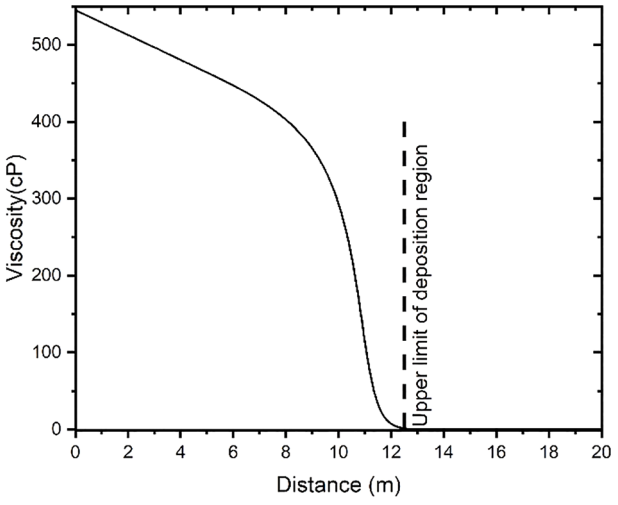

Fig. 6. Viscosity vs. distance (at 1.37 yrs): Depletion example.

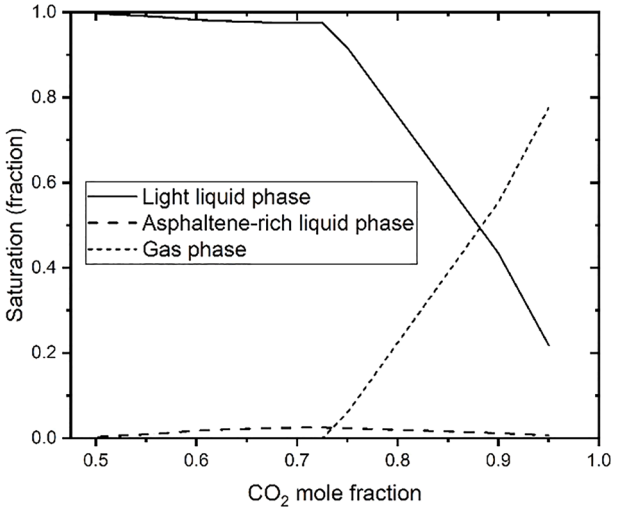

Fig. 7. Saturation of the three phases vs. CO2 overall mole fraction in Weyburn oil, P = 160 bar, T = 332 K: CO2 injection example.

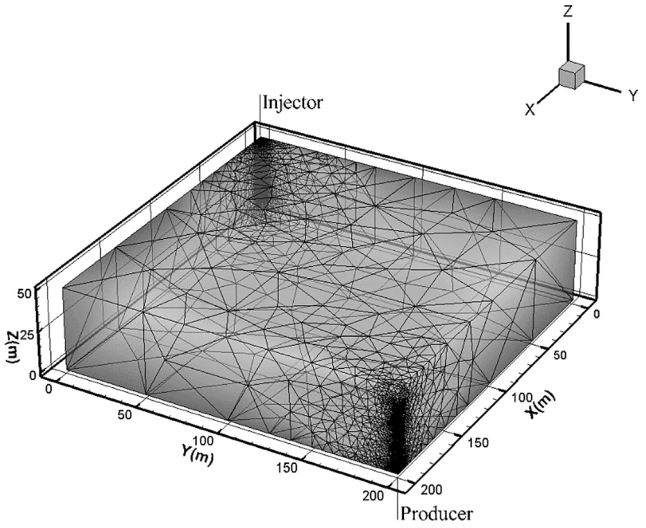

Fig. 8. Domain showing the injection and production wells: CO_2 injection example.

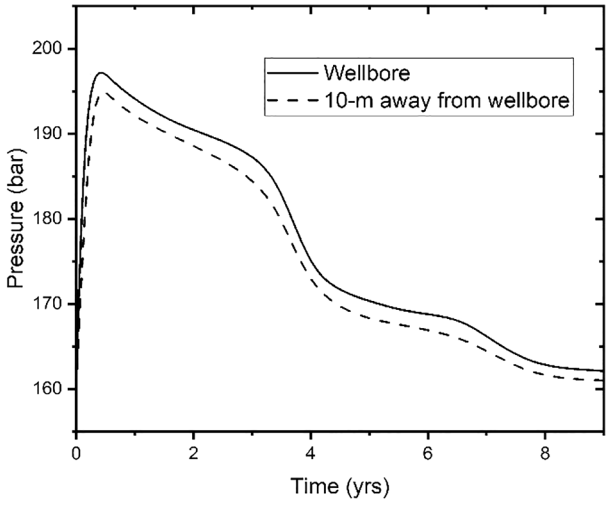

Fig. 9. Pressure vs. time at the injector wellbore and 10-m away from the wellbore: CO_2 injection example.

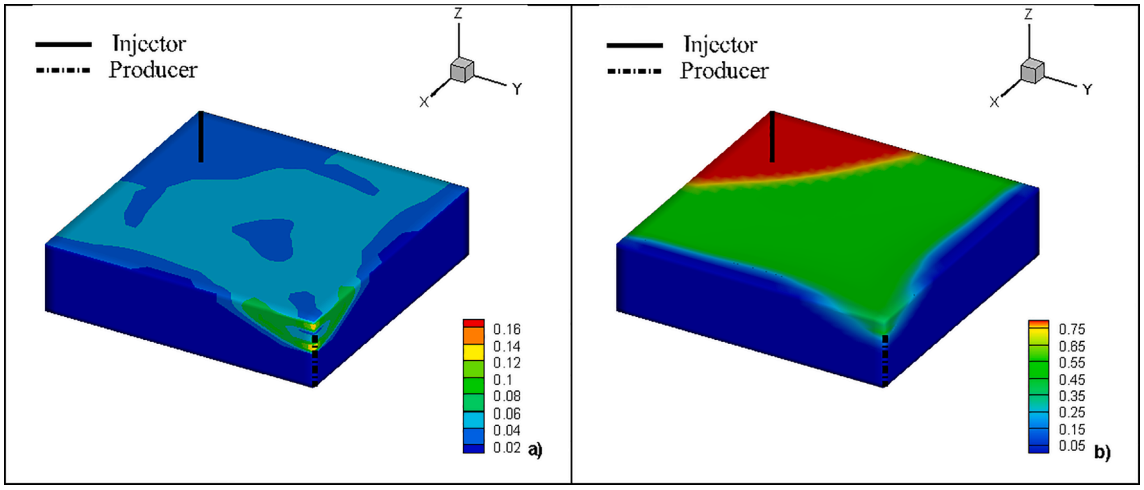

Fig. 10. Saturation of asphaltene-rich liquid phase (fraction) (a), and gas phase (fraction) (b) (at 5.5 yrs): Note that asphaltene-rich liquid phase saturation in (a) has a lighter color than regions without asphaltene shown in dark blue: CO_2 injection example. (For interpretation of the references to color in this figure legend, the reader is referred to the web version of this article.)

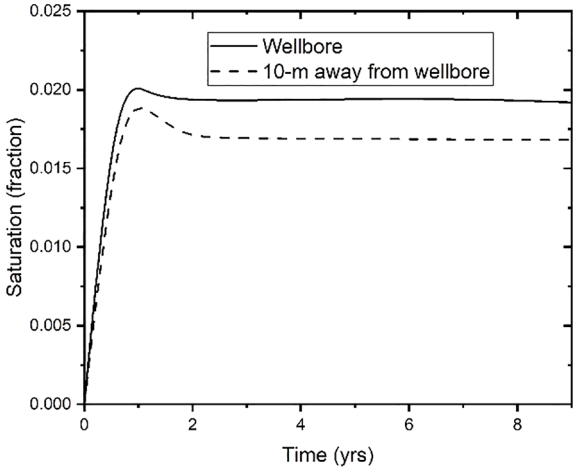

Fig. 11. Saturation of asphaltene-rich liquid phase at the top (first layer of grids in contact with the top perforation) vs. time at the Injector wellbore and 10-m away from the wellbore: CO_2 injection example.

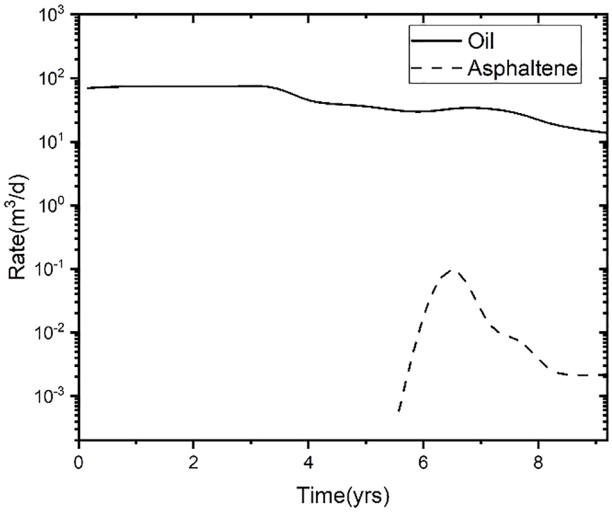

Fig. 12. Oil and asphaltene-rich phase production rate vs. time: CO_2 injection example.

water was not established, and we used an end point value of unity. We assume 20% irreducible water saturation in the field scale. The initial reservoir pressure is 500 bar at the bottom of the formation. The effect of gravity is considered in this example as opposed to the lab scale, in which a thin tube was used. A vertical 40 m-long well at a production rate of 30 m^3/day is located at the center of the reservoir with the well head located at the top of the formation. Only 35 m of the total well length is assumed to be perforated. More details about our well modeling approach are presented in our recent paper [24]. The domain and the mesh discretization near the well region are shown in Fig. 4. The total number of grids is 24,516 tetrahedrons.

In our simulations, the production rate is gradually increased over a period of two weeks. The pressure is decreased at the well from an initial value near 500 bar. In Fig. 5a we show the pressure vs. time at the well boundaries and at different distances from the well. As shown in Fig. 5b, the deposition forms at the well boundary when the pressure reaches the AOP. The deposition increases the rate of pressure drop, in turn leading to asphaltene deposition away from the well boundary. The saturation of the asphaltene-rich liquid phase reaches a high value (16%) at 1.38 yrs which results in a decrease of oil production rate. At this point, the first part of the simulation ends. In the second part of the simulation (around 1.38 yrs), the asphaltene-rich liquid phase is removed from the 10-m region of the well by assigning a value of zero to the saturation of the asphaltene-rich liquid phase. To the best of our knowledge there are no presentations in the literature on formation and removal of asphaltene in the wellbore from compositional simulations. One advantage of the proposed approach is the ease to accomplish this simulation without the need to account for adsorption and/or mechanical plugging. Asphaltene removal is achieved in one step, however the pressure is systematically controlled after the removal for a period of 10 days by allowing small changes during this period (Fig. 5a). As asphaltene starts to deposit in the second cycle, the well pressure decreases. The second cycle continues to 1.8 yrs and is stopped before further deposition occurs and to avoid production loss. The higher rate of deposition in the second cycle is noticeable compared to the first cycle. In another simulation (results not shown) we remove the asphaltene phase within 5-m of the wellbore and results similar to those shown in Fig. 5 are obtained. In Fig. 6 we show the viscosity of the asphaltene-rich phase at different distances from the wellbore at 1.38 yrs; the plot shows no significant depositions further than 10-m from the wellbore and no deposition is observed more than 13-m away from the wellbore. After the asphaltene is removed (Fig. 5b), it starts to re-deposit in the second cycle of the simulation and

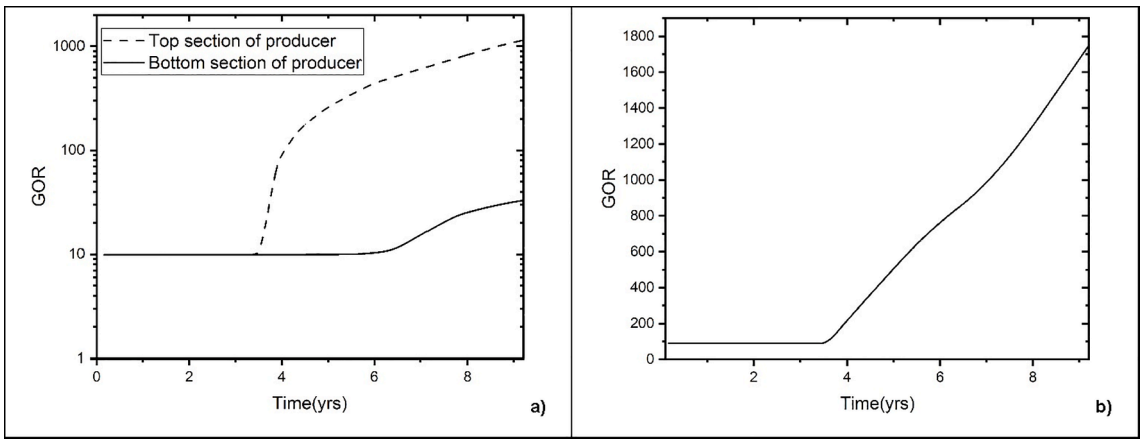

Fig. 13. GOR vs. time at the top and bottom sections of the producer (a), and the overall GOR (b): CO_2 injection example.

Table A1
Composition of the phases in mole fraction.

Component	Gas phase	Light liquid phase	Asphaltene-rich liquid phase
CO_2	0.9489	0.7359	0.5831
$N_2/H_2S/C_1$	0.0232	0.0134	0.0066
C_2-C_3	0.0161	0.0196	0.0173
C_4-C_5	0.0069	0.0128	0.0115
Heavy fraction	0.0049	0.2181	0.2586
Asphaltene	0	0.0002	0.1229

Table A2
EOS parameters for characterization of Weyburn oil.

Component	T_c[K]	P_c[bar]	Acentric	Molar weight[g/mol]
CO_2	304.14	73.75	0.239	44.01
$N_2/H_2S/C_1$	191.83	47.08	0.024	20.66
C_2-C_3	350.44	44.35	0.136	39.89
C_4-C_5	448.30	35.15	0.223	66.72
Heavy fraction	746.22	15.91	1.004	220.10
Asphaltene	1474	6.34	2.	1800

Association volume: 0.01; Association energy for asphaltene-asphaltene: 2000 K; Association energy for asphaltene-resin: 500 K.

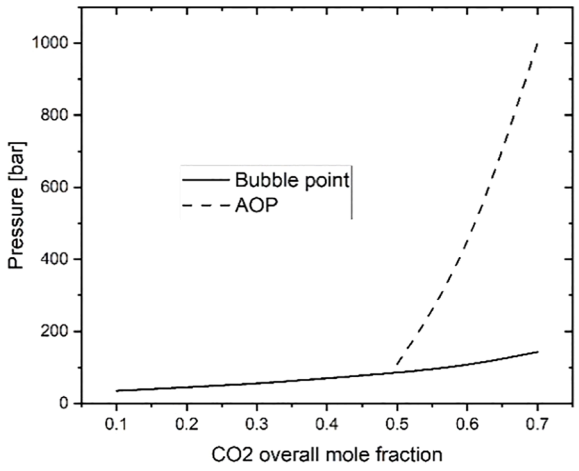

Fig. A1. AOP and bubble point pressure as a function of CO_2 overall mole fraction.

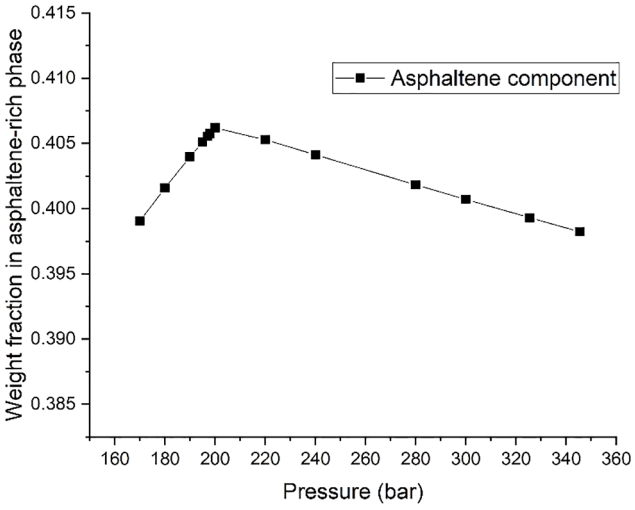

Fig. A2. Asphaltene content of asphaltene-rich phase vs pressure; Live oil.

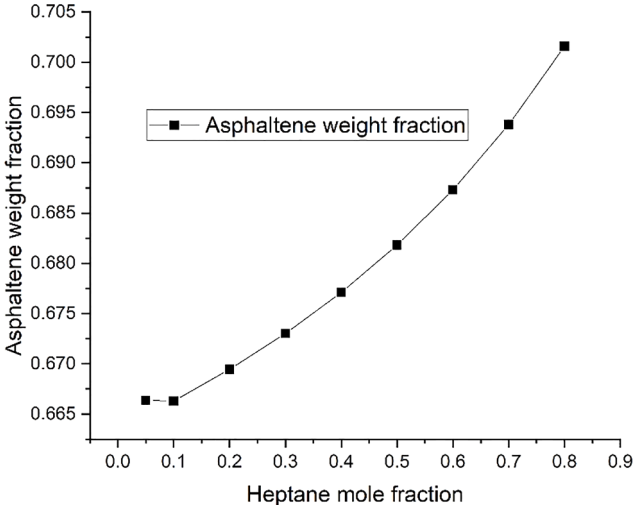

Fig. A3. Asphaltene content of asphaltene-rich phase vs heptane mixing in mole fraction: STO.

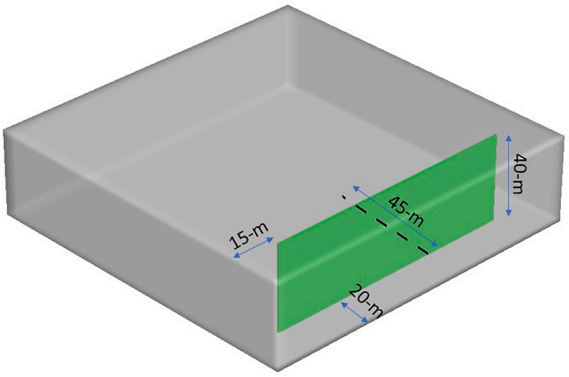

Fig. B1. Horizontal well crossing a vertical fracture.

reaches a value of 13% around the wellbore after about 9 weeks of production. Note that when asphaltene saturation exceeds 10%, a small amount of the asphaltene-rich liquid phase will be produced with the oil. In the next example we will present asphaltene phase production. Fig. 6 clearly demonstrates that because of the transfer of the lighter components from asphaltene-rich phase to oil phase at lower pressure, there is a drastic increase of viscosity and very low mobility of the asphaltene-rich liquid phase and a sharp build-up close to the well. In Appendix B we present the results of asphaltene deposition in formation around a well which crosses a fracture. The asphaltene saturation in the fracture is higher than the matrix indicating a significant effect on well performance.

3.3. *Asphaltene deposition in reservoir from CO_2 injection*

In this example we consider injection of CO_2 in a reservoir saturated with Weyburn oil [32] which has a small fraction of light components. Srivastava et al. [33] show that asphaltene precipitates when CO_2 is mixed with this oil. There is asphaltene precipitation from CO_2 mixing with the reservoir fluid. In Fig. 7 we show the saturation of the phases (gas, light liquid phase and asphaltene-rich liquid phase) as a function of CO_2 mole fraction. The pressure and temperature are 160 bar and 332 K, respectively. The injection rate is 500 sm^3/day, and production is performed at constant pressure. The reservoir fluid characterization is from [32]. The simulation domain and all relevant data are the same as in the previous example, the main difference being that there are two wells, an injector, and a producer. Discretization grids (total of 36,542 tetrahedrons) and locations of injection and production wells are shown in Fig. 8. The top of injector is at the top of the formation and the bottom of the producer intersects with the bottom of the formation. Both wells have the same length.

In Fig. 9 we show the pressure at the wellbore (injector) and 10-m away from the wellbore as a function of time. Pressure profiles show a sharp increase at the beginning of injection due to asphaltene deposition

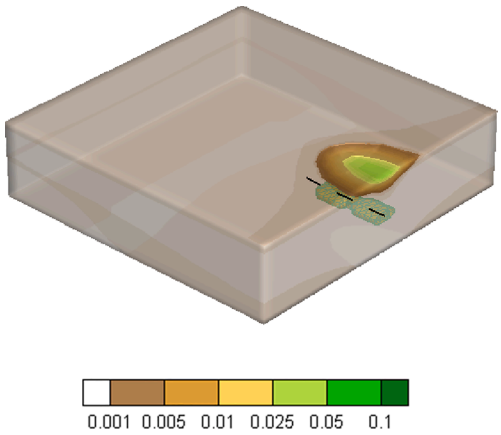

Fig. B3. Asphaltene-rich phase saturation without the fracture.

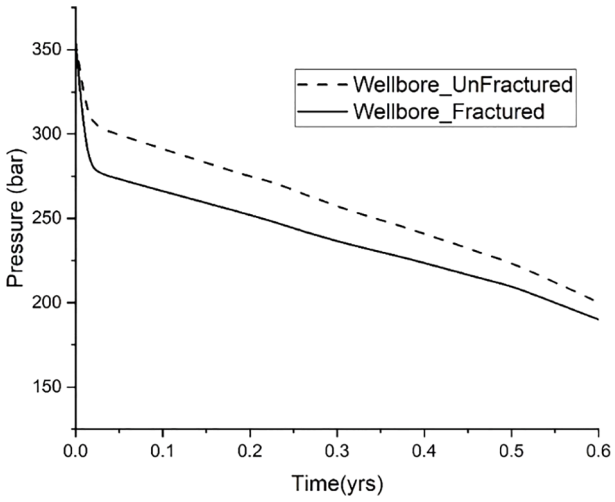

Fig. B4. Pressure in the well vs time with and without the vertical fracture.

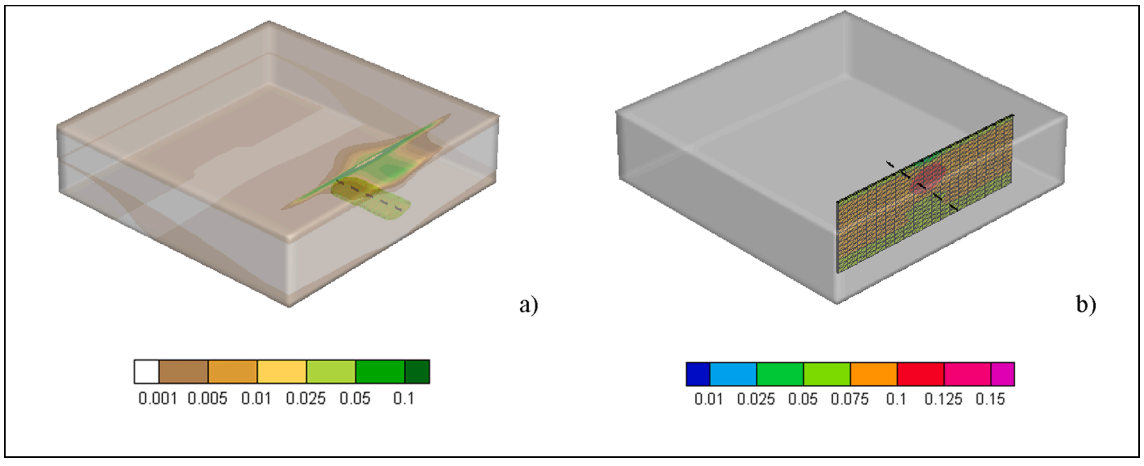

Fig. B2. Asphaltene-rich phase saturation in the matrix (a) and the fracture (b). Note change of color code in representation of asphaltene-rich phase saturation in the fracture and the matrix.

and change of composition. The pressure starts to decrease as CO_2 starts to dissolve into oil and from production. After a few months, pressure starts a decreasing trend due to the decrease in asphaltene phase saturation. A sharp decrease in pressure at the injection well and near the wellbore region is observed around 3.8 yrs at breakthrough time. At this time, the asphaltene starts to deposit at the top of the producer and the top corner of the reservoir near the producer. The maximum saturation of asphaltene phase in this region is in the range of 14% as shown in Fig. 10a. The high asphaltene-rich liquid phase saturation at the top results from a lower density of CO_2 than the oil phase and much lower viscosity. The asphaltene phase in Weyburn oil precipitates when the composition of CO_2 in the oil phase exceeds 45% from direct mixing at 160 bar and 332 K. The saturation of the asphaltene-rich liquid phase around the injector and throughout the reservoir (except for the producer and near-producer region) does not exceed 2%. For reference we show in Fig. 11 the variation of saturation of the asphaltene-rich liquid phase at the injector and 10-m away from the injector as functions of time. The effect of deposition around the producer well on production rate is shown in Fig. 12. The oil rate increases to reach a maximum value until a sharp decrease is observed at breakthrough time. Because the critical asphaltene-rich liquid phase saturation is assumed to be10%, no asphaltene-rich phase is produced before 5.5 yrs. At 5.5 yrs the asphaltene-rich liquid phase saturation exceeds 10% and asphaltene phase is produced in the well, reaching a maximum within one year (i.e., at 6.5 yrs) and declining afterwards. Note that the production of the asphaltene liquid phase is very small compared to the oil phase rate. The high viscosity near the well bore results in very low mobility. The decrease of production in oil phase and asphaltene-rich phase is due to the increase in gas production rate. There is a so-called "second breakthrough" which affects the pressure profile when the second slope decrease is observed. In Fig. 13 we show the GOR at the top and the bottom sections of the producer in addition to the overall GOR. The top and bottom sections are based on the grids that are in contact with the well boundary. The breakthrough occurs when gas is produced from the top perforations of the well. Gravity causes gas to reach the top section first. The second breakthrough occurs when the gas phase reaches the bottom section of the well.

4. Conclusion

We have demonstrated that asphaltene deposition in porous media can be described without the need to include complexities such as adsorption and pore plugging commonly used in the literature. The relative permeability concept accounts for adsorption and small pore plugging in two-phase flow of asphaltene-rich liquid phase and an asphaltene-lean liquid phase. In the comprehensive set of lab measurements in [30], connate water was not established in the porous media. There are various deposition measurements in flow lines and on asphaltene particle size measurements [31,34,35] that show a pronounced effect of water. One may perform analysis of lab scale experiments with connate water to infer the relative permeability of the oil phase and the asphaltene-rich liquid phase.

The main conclusions of this work are:

- At reservoir scale depletion, there is a drastic effect of asphaltene precipitation on pressure at the wellbore in the producer at constant production rate.
- Using a realistic representation of the well geometry, it is shown that asphaltene deposition is observed only in a small region close to the wellbore.
- To increase well production performance, intervention is needed every few weeks to remove (by dissolution or other means) the deposited asphaltenes which may be limited to a small region where asphaltene is deposited.
- In CO_2 injection when there is deposition, the asphaltene-rich saturation gradually decreases in the injection wellbore resulting in injection pressure decrease at constant injection rate. Results show the maximum saturation of asphaltene-rich liquid phase is observed at the producer and near the producer region.
- In the producer there may be a very low production rate of asphaltenes from the reservoir to the well. In one of the examples in this work, the production of asphaltene-rich liquid phase is about three orders of magnitude less than that of the oil phase. Despite very low rate it can accumulate over time. There is need to remove the asphaltene-rich liquid phase in the well and around wellbore from time to time.

CRediT authorship contribution statement

Ali Zidane: . **Abbas Firoozabadi:** Supervision.

Declaration of Competing Interest

The authors declare that they have no known competing financial interests or personal relationships that could have appeared to influence the work reported in this paper.

Acknowledgement

This work was supported by the member companies of the Reservoir Engineering Research Institute (RERI) whose support is gratefully acknowledged.

Appendix A

For reference we show in Table A1 the compositions of the three phases (gas, oil and asphaltene-rich) at 160 bar and 332 K in the Weyburn oil. The compositions (in mole fraction) are based on a 75% overall mole fraction of CO_2. The amount of CO_2 in the asphaltene-rich liquid phase is significant.

In Table A2 we show the EOS parameters used in the characterization of Weyburn oil. The binary interaction coefficients (BIC) are as follows. For hydrocarbon-CO_2 a value of 0.071 is used and for hydrocarbon-C_1, the BIC is calculated based on the molar weight using the equation below:

$$\mathrm{BIC of hydrocarbon} - \mathrm{C1} = 0.0289 + 1.633 M_w 10^{-4} \quad (1)$$

All the other BICs are set to zero.

In Fig. A1 we show the variation of upper AOP and bubble point pressure as a function of CO_2 overall mole fraction. Note that no asphaltene deposition is observed for CO_2 overall mole fraction less than 45%.

We show in Fig. A2 the weight fraction of the asphaltene component in the asphaltene-rich phase as a function of pressure. The oil composition is given in Table 1 in the text. Results show the asphaltene content reaches a maximum slightly above 40 wt%. Mixing the STO of the same oil with heptane at various ratios shows an increase of the weight fraction up to 70% as shown in Fig. A3. The large different in asphaltene content of the asphaltene-rich phases from pressure effect in a live oil and mixing of STO with heptane may have significant implications in flow. The former may be treated as a phase which will flow.

Appendix B

In this appendix we present simulation results of formation depletion and asphaltene deposition where a horizontal well intersects a vertical fracture (Fig. B1). Relevant data of the domain are from the depletion example in the text. The fracture permeability is 100 d and the aperture is 2 mm and the matrix permeability is 50 md.

In Fig. B2 we show the asphaltene-rich phase saturation in the matrix and in the fracture including the wellbore. Fig. B3 shows the simulation shows for the corresponding unfractured well. The variation of the pressure with respect to time in both cases (with and without the vertical fracture) are shown in Fig. B4. Results show the effect of the fracture on the pressure due to the accumulation of deposited asphaltene. Fig. B2 reveals higher asphaltene-rich phase saturation in the fracture than in the matrix.

References

[1] Firoozabadi A. Thermodynamics and Applications of Hydrocarbons Energy Production. McGraw-Hill Professional; 2015.

[2] Buckley JS. Asphaltene precipitation and crude oil wetting. Society of Petroleum Engineers 1995. https://doi.org/10.2118/26675-PA.

[3] Kamath VA, Yang J, Sharma GD. Effect of asphaltene deposition on dynamic displacements of oil by water. Society of Petroleum Engineers. 1993. https://doi.org/10.2118/26046-MS.

[4] Clementz DM. Alteration of rock properties by adsorption of petroleum heavy ends: implications for enhanced oil recovery. Society of Petroleum Engineers 1982. https://doi.org/10.2118/10683-MS.

[5] Nghiem LX, Coombe DA, Ali SMF. Compositional simulation of asphaltene deposition and plugging. Society of Petroleum Engineers 1998. https://doi.org/10.2118/48996-MS.

[6] Kohse BF, Nghiem LX. Modelling asphaltene precipitation and deposition in a compositional reservoir simulator. Society of Petroleum Engineers 2004. https://doi.org/10.2118/89437-MS.

[7] Wang S, Civan F. Modeling formation damage by asphaltene deposition during primary oil recovery. J Energy Resour Technol 2005;127(4):310–7. https://doi.org/10.1115/1.1924465.

[8] Jafari Behbahani T, Ghotbi C, Taghikhani V, Shahrabadi A. Investigation on asphaltene deposition mechanisms during CO2 flooding processes in porous media: a novel experimental study and a modified model based on multilayer theory for asphaltene adsorption. Energy Fuels 2012;26(8):5080–91. https://doi.org/10.1021/ef300647f.

[9] Mohebbinia S, Sepehrnoori K, Johns RT, Kazemi Nia Korrani A. Simulation of asphaltene precipitation during gas injection using PC-SAFT EOS. J Petrol Sci Eng 2017;158:693–706.

[10] Abouie A, Tagavifar M, Sepehrnoori K. Wettability alteration and flow coupling in gas flooding of asphaltenic reservoirs. Society of Petroleum Engineers 2018. https://doi.org/10.2118/190295-MS.

[11] Chapman WG, Gubbins KE, Jackson G, Radosz M. SAFT: equation-of-state solution model for associating fluids. Fluid Phase Equilib 1989;52:31–8. https://doi.org/10.1016/0378-3812(89)80308-5.

[12] Jin Z, Firoozabadi A. Flow of methane in shale nanopores at low and high pressure by molecular dynamics simulations. J Chem Phys 2015;143(10):104315. https://doi.org/10.1063/1.4930006.

[13] Jiménez-Ángeles F, Khoshnood A, Firoozabadi A. Molecular dynamics simulation of the adsorption and aggregation of ionic surfactants at liquid-solid interfaces. J Phys Chem C 2017;121(46):25908–20. https://doi.org/10.1021/acs.jpcc.7b09466.

[14] Nasrabadi H, Moortgat J, Firoozabadi A. New three-phase multicomponent compositional model for asphaltene precipitation during CO2 injection using CPA-EOS. Energy Fuels 2016;30(4):3306–19. https://doi.org/10.1021/acs.energyfuels.5b02944.

[15] F.A. Gonzalez, D.L. Gonzalez, B. Altemeemi, A. Al-Nasheet, F. Snasiri, S. Jassim, S. Sinha, P. Shaw, E. Ghloum, B. Al-Kandari, S. Kholosy, A. Emadi, Understanding of Asphaltene Deposition in the Production Tubing and Reservoir Rock While Flowing at Bottom-Hole Pressure Below Asphaltene Onset Pressure, AOP in the Magwa-Marrat Field. Paper presented at the SPE Kuwait Oil & Gas Show and Conference, Mishref, Kuwait, October 2019. doi: 10.2118/198121-MS.

[16] Huggenberger P, Zidane A, Zechner E, Gechter D. The role of tectonic structures and density-driven groundwater flow for salt karst formation. Eng Geol Soc Territory 2015;5:609–12.

[17] Younes A, Fahs M, Belfort B. Monotonicity of the cell-centered triangular MPFA method for saturated and unsaturated flow in heterogeneous porous media. J Hydro 2013;504:132–41.

[18] Younes A, Fahs M, Zidane A, Huggenberger P, Zechner E. A new benchmark with high accurate solution for hot–cold fluids mixing. Heat Mass Transf 2015;51(9):1321–36.

[19] Hoteit H, Firoozabadi A. Numerical modeling of diffusion in fractured media for gas injection and recycling schemes. SPE J 2009;14(2):323–37. https://doi.org/10.2118/103292-PA. SPE-103292-PA.

[20] Moortgat J, Firoozabadi A. Mixed-hybrid and vertex-discontinuous-Galerkin finite element modeling of multiphase compositional flow on 3D unstructured grids. J Comput Phys 2016;315:476–500.

[21] Zidane A, Firoozabadi A. Fracture-cross-flow equilibrium in compositional two-phase reservoir simulation. Society of Petroleum Engineers 2017:950–70. https://doi.org/10.2118/184402-PA.

[22] Zidane A, Firoozabadi A. Reservoir simulation of fractured media in compressible single-phase multicomponent in 2D, 2.5 D and 3D unstructured gridding. Adv Water Resour 2018;121:68–96. https://doi.org/10.1016/j.advwatres.2018.08.005.

[23] Zidane A, Firoozabadi A. Efficient simulation of two-phase compositional flow in fractured reservoirs using 3D unstructured gridding in complex geometries. Society of Petroleum Engineers 2018. https://doi.org/10.2118/191405-MS.

[24] Zidane A, Firoozabadi A. Two-phase compositional flow simulation in complex fractured media by 3D unstructured gridding with horizontal and deviated wells. SPE Reservoir Eval Eng 2020. https://doi.org/10.2118/191405-PA.

[25] Stone HL. Probability model for estimating three-phase relative permeability. J Petrol Technol 1970;23(2):214–8.

[26] Stone HL. Estimation of three-phase relative permeability and residual oil data. J Can Pet Technol 1973;12(4):53–61.

[27] L.E. Baker, Three-phase relative permeability correlations. SPE Enhanced Oil Recovery Symposium, Tulsa, OK, 1988, 16-21.

[28] Li K, Firoozabadi A. Experimental study of wettability alteration to preferential gas-wetting in porous media and its effects. SPE Res Eval & Eng 2000:139–49. https://doi.org/10.2118/62515-PA.

[29] Tang GQ, Firoozabadi A. Gas- and liquid-phase relative permeabilities for cold production from heavy-oil reservoirs. SPE Res Eval & Eng 2003:70–80. https://doi.org/10.2118/83667-PA.

[30] Mohammadzadeh O, Taylor SD, Eskin D, Ratulowski J. Experimental investigation of asphaltene induced formation damage due to pressure depletion of live reservoir fluids in porous media. Society of Petroleum Engineers 2017. https://doi.org/10.2118/187053-MS.

[31] Hashmi SM, Firoozabadi A. Effect of dispersant on asphaltene suspension dynamics: aggregation and sedimentation. J Phys Chem B 2010;114:15780–8.

[32] Li Z, Firoozabadi A. Modeling asphaltene precipitation by n-alkanes from heavy oils and bitumens using cubic-plus-association equation of state. Energy&Fuels 2010;24(2):1106–13.

[33] Srivastava RK, Huang SS, Dong M. Asphaltene deposition during CO2 flooding. Society of Petroleum Engineers 1999. https://doi.org/10.2118/59092-PA.

[34] Aslan S, Firoozabadi A. Effect of water on deposition, aggregate size, and viscosity of asphaltenes. Langmuir 2014;30(13):3658–64.

[35] T. Kar, K. Naderi, A. Firoozabadi, Asphaltene deposition and removal in flowlines and mitigation by effective functional molecules. 2020, SPE 199878.